J. KSIAM Vol.13, No.2, 123–140, 2009

A COMPUTATIONAL MODEL FOR OSMOSIS PHENOMENA OF CELLS THROUGH SEMI-PERMEABLE MEMBRANES

IMBUNM KIM[1], TAEYOUNG HA[2], AND DONGWOO SHEEN[1,3†]

[1]DEPARTMENT OF MATHEMATICS, SEOUL NATIONAL UNIVERSITY, SEOUL 151-747, KOREA
E-mail address: {ikim, sheen}@snu.ac.kr

[2]NATIONAL INSTITUTE FOR MATHEMATICAL SCIENCES, DAEJEON 305-340, KOREA
E-mail address: tha@nims.re.kr

[3]INTERDISCIPLINARY PROGRAM IN COMPUTATIONAL SCIENCE & TECHNOLOGY, SEOUL NATIONAL UNIVERSITY, SEOUL 151-747, KOREA

ABSTRACT. The effect of a solute concentration difference on the osmotic transport of water through the semi-permeable membrane of a simple cell model is investigated. So far, most studies on osmotic phenomena are described by simple diffusion-type equations ignoring all fluid motion or described by Stokes flow. In our work, as the governing equations, we consider the coupled full Navier-Stokes equations which describe the fluid motion and the full transport equation that takes into account of convection and diffusion effects. A two dimensional finite difference model has been developed to simulate the velocity field, concentration field, and semi-permeable membrane movement. It is shown that the cell swells to regions of lower solute concentration due to the uneven water flux through the semi-permeable membrane. The simulation is applied on a red blood cell geometry and the relevant results are presented.

1. INTRODUCTION

The phenomena of osmosis, reverse osmosis, and electro-osmosis are of considerable importance in both life and physical sciences and they involve the separation of gaseous and liquid mixtures through semi-permeable membranes. Reverse osmosis is an energy efficient technique for separating liquid solutions and gas mixtures and can be applied in the field of water purification, chemical, electro-chemical, biochemical, radioactive waste treatment, and food processing [20]. Electro-osmosis can be defined as the effect of an external electric field on an osmosis and reverse osmosis system. It has been widely used in many applications such as dewatering, contaminant transport mitigation, fluid transport in eyes [9, 19]. Osmosis is of great importance in biological and medical processes where the solvent is water. The transport of water and other molecules across biological membranes is essential to many processes

Received by the editors May 8 2009; Accepted May 25 2009.
2000 *Mathematics Subject Classification.* 76Z99, 65N06.
Key words and phrases. Osmosis, natural convection model, level set method, red blood cell.
† Corresponding author.

in living organisms. When the extracellular solution is highly concentrated compared to the intracelluar part, *i.e.,* when the cells are in hypertonic condition, more water molecules pass osmotically from the inside to the outside of the cell than the water molecules passing inward to the cell; as a result, the cells dehydrate and shrink. On the other hand, if cells are placed in hypotonic solution, then more water molecules from the extracellular region move into the cell than the water molecules get out; in these circumstances, the cells swell with the excess water and eventually burst open. If cells are in isotonic condition in the extracellular fluids, this results in an equilibrium between osmosis into the cell and out of the cell. Cells respond most positively to this kind of extracellular fluid. This intricate balance in osmosis in and out of the cells needs to be maintained at all times. An obvious application of this phenomenon is the development of protocols for the cryopreservation of living cells. The cryopreservation of living cells depends on the ability of cells to survive osmotic stress, which may be seriously imposed during freezing and thawing protocols [4]. The main questions are about the success of freezing and thawing process related to the irreversibility of membrane structural changes after thawing [17], the localization of cryoprotectant in internal and external cell membranes, the intracellular structural changes following cryopreservation and reasons for the need to impose different kinetics in thawing and freezing [12, 13]. All of these questions require a complete understanding of water and solute transport into and out of cells in hypertonic or hypotonic conditions.

Researches on these topics were performed mostly in the experimental fields [22, 8, 10]. A few molecular level simulations of osmosis, reverse osmosis and electro-osmosis in fluid mixtures using semi-permeable membranes are reported [14, 11, 15]. All the molecular level simulations were carried out using the molecular dynamics simulation which basically solves ordinary differential equations and conclude solutions in molecular level. Very recently, a macroscopic approach to get solutions has been reported for these phenomena. Khan and Reppert [6] simulated the PDEs for the electro-osmosis model in a closed channel using the finite element method and compared them to analytical solutions. In their work, the geometry is fixed without introducing any interface, which makes it easy to simulate. Kirichenko [7] considered the features of mass transfer in a horizontal nonflow-through-reverse-osmosis cell. From the set of the NS equations in the Boussinesq approximation, a set of ordinary differential equations for perturbations is derived by the normal mode method in the case of the exponential concentration profile and it is solved numerically. In contrast, in spite of its importance, there is little numerical study for osmosis phenomena. In this paper, we are going to focus on the study of osmosis especially in the macroscopic level.

In the theoretical and numerical study for osmosis initiated by Pedley in 1982 [16]. the author studied the phenomenon of a natural convection driven by osmosis through a vertical non-moving semi-permeable membrane and derived simple approximate formula for estimating the total osmotic flux across a membrane and the results are interpreted in the light of experiments to measure osmotic permeability. In general, the cell and the ambient fluid are moving and one must solve for both the fluid motion and the distribution of the solute concentration. The solute is advected by the fluid flow, and the solute can influence the fluid motion through the change in buoyancy force as well as surface tension. However, surface tension

effects are difficult to determine. The simplest mathematical model of the response of a cell to varying solute concentration in the surrounding fluid is to assume that the fluid motion remains zero and ignore all mechanical properties of the cell membranes. For initially uniform solute concentration, Batycky *et al.* showed that the fluid velocity is zero while a cell changes its volume due to the osmotic flow of water through its interfaces. For nonuniform and time dependent concentration, the cells were modeled as small sacs filled with homogeneous medium [2]. Jaeger *et al.* [5] assumed that the cells are modeled as simple vesicles, the intracellular and extracellular medium is a binary solution, the solute is completely nonpermeating, the membrane has constant properties, no fluid motion is induced by membrane forces or density variations, and no cell motion is induced by gravity. However, their assumptions are too simple to describe the nature of the cells and transport properties of cell membrane. To study more accurate interaction phenomena of cells, we have to determine the hydrodynamic velocity field induced by the diffusion process, simultaneously with the solution of the concentration field which reflects highly nonlinear behaviors owing to the coupling of these fields.

Anderson [1] introduced the Stokes equations which the fluids inside and outside obey for a rigid spherical vesicle and obtained an expression for the osmophoretic velocity. This velocity is proportional to the concentration gradient but it is independent of the fluid viscosity. Zinemanas *et al.* [23] applied this to deformable membranes, but using a simple Laplacian equation for the concentration field. To our knowledge, no computational studies on solving the coupled velocity and concentration fields have been achieved and reported about osmotic phenomena. In this paper, we take into account the coupled Navier-Stokes equations which contain not only the density variations but also gravity to describe fluid motion, and the full transport equation that consists of convection and diffusion effects. The mathematical formulation and underlying physics are presented in Sect 2. The equations are written in dimensionless form and characteristic numbers(Grashof, Schmidt) are introduced. The numerical method used in our computation is presented in Sect 3. Results from our simulation is addressed in Sect 4. Conclusions follow in Sect 5.

2. MATHEMATICAL MODELING

In this study, we consider the natural convection fluid motion in a cell and its surrounding media driven by osmosis through a semi-permeable membrane in a bounded computational domain. The computational domain is a two or three dimensional space with the space and time variables $\mathbf{x}$ and t. $\psi(\mathbf{x}, t)$ represents the continuous volumetric density field (such as mass density $\rho(\mathbf{x}, t)$, concentration $c(\mathbf{x}, t)$). The total amount of the property $\Psi(t)$ within the control volume $\Omega(t)$ is given by

$$\Psi(t) \equiv \int_{\Omega(t)} \psi(\mathbf{x}, t) dV.$$

For moving interface, the Reynolds transport theorem can be stated as

$$\frac{d\Psi}{dt} = \int_{\Omega(t)} \left(\frac{\partial \psi}{\partial t} + \mathbf{u}_f \cdot \nabla \psi \right) d\Omega + \int_{S(t)} (\mathbf{u}_m - \mathbf{u}_f) \psi \cdot d\mathbf{S}, \tag{2.1}$$

which is a sum of contributions from the time rate change of ψ within V, convection of ψ across the membrane at the fluid velocity $\mathbf{u}_f$, and transport of ψ across the membrane due to the difference in the fluid and membrane velocities $\mathbf{u}_m$. Now, we take $\psi(\mathbf{x},t) = c(\mathbf{x},t)$, then $\Psi(t) = N(t)$ is the total number of moles of solute in each phase. The concentration field $c(\mathbf{x},t)$ satisfies the following convection diffusion equation:

$$\frac{\partial c}{\partial t} + \mathbf{u}_f \cdot \nabla c = D\nabla^2 c, \tag{2.2}$$

with the diffusion constant D. By using Equations (2.1) and (2.2), the Divergence Theorem yields

$$\frac{dN}{dt} = A\left[D\frac{\partial c}{\partial \nu} + \nu \cdot (\mathbf{u}_m - \mathbf{u}_f)c\right], \quad \mathbf{x} \in \partial\Omega. \tag{2.3}$$

Here, A denotes the area of the cell and ν the unit outward normal to the cell, and thus $\nu \cdot \mathbf{u}_m$ and $\nu \cdot \mathbf{u}_f$ represent the outward normal components of the velocities $\mathbf{u}_m$ and $\mathbf{u}_f$ to $\partial\Omega$, respectively. Since the membrane is impermeable to solute, the solute flux across the membrane is always zero. Therefore, Equation (2.3) gives the interface condition on c at the membrane interface:

$$D\frac{\partial c}{\partial \nu} + \nu \cdot (\mathbf{u}_m - \mathbf{u}_f)c = 0, \quad \mathbf{x} \in \partial\Omega, \tag{2.4}$$

With the transport equation for concentration field, the equations of mass and motion of incompressible fluid are given as follows:

$$\nabla \cdot \mathbf{u}_f = 0, \tag{2.5}$$

$$\frac{\partial \mathbf{u}_f}{\partial t} + (\mathbf{u}_f \cdot \nabla)\mathbf{u}_f = \frac{\mu}{\rho}\nabla^2 \mathbf{u}_f - \frac{\nabla p}{\rho} + \mathbf{g}, \tag{2.6}$$

where ρ, μ and $\mathbf{g}$ are the fluid density, dynamic viscosity, and gravitational force, respectively. Consider a free convection system in which the fluid concentration varies about some bulk value c_B. If the fluid is at c_B and the fluid does not move, the pressure gradient in the system is given by the equation of motion with $\mathbf{u}_f = 0$. This implies

$$\nabla p = \rho(c_B)\mathbf{g}. \tag{2.7}$$

If the velocity gradient results entirely from concentration differences, the fluid motion is usually quite slow, and therefore Equation (2.7) may be assumed to be a reasonably good approximation of the pressure gradient even in the moving fluid. With this assumption, we expand ρ by a Taylor series in c about bulk concentration c_B,

$$\begin{aligned} \rho &= \rho(c_B) + (\frac{d\rho}{dc})_{c_B}(c - c_B) + \cdots \\ &= \rho(c_B) + \beta\rho(c_B)(c_B - c) + \cdots . \end{aligned}$$

Here, we have introduced the coefficient of volume expansion β evaluated at c_B. This is defined by $\beta = \frac{1}{V}(\frac{\partial V}{\partial c}) = \frac{1}{1/\rho}(\frac{\partial(1/\rho)}{\partial c}) = -\frac{1}{\rho}(\frac{\partial \rho}{\partial c})$. By substituting all assumptions, we may express

Equation (2.6) as

$$\frac{\partial \mathbf{u}_f}{\partial t} + (\mathbf{u}_f \cdot \nabla)\mathbf{u}_f = \frac{\mu}{\rho(c_B)}\nabla^2 \mathbf{u}_f + \frac{\mathbf{g}}{\rho(c_B)}(\frac{d\rho}{dc})_{c_B}(c_B - c). \tag{2.8}$$

This is the equation of motion used in free convection when a bulk concentration c_B is defined and it is also limited to low fluid velocities and small concentration variations.

The driving force for membrane motion is a difference in net osmotic pressure on both membrane sides. This osmotic pressure is defined as

$$\Pi = cRT,$$

where R is the universal gas constant and T is the absolute temperature. For an observer fixed on the membrane, the water passes through the membrane with velocity $-\mathbf{u}_m$. The osmotic pressure and the stress field differences across the membrane induce a normal solvent osmotic velocity relative to the membrane as given by [1]

$$\nu \cdot \mathbf{u}_m = -LRT(c_f - c_c) = -LRT\Delta c,$$

where c_f and c_c represent the extracellular and intracellular solute concentrations, L is a hydraulic permeability. Note that the van't Hoff osmotic term is valid for low solute concentrations and that the normal stress is used instead of the pressure difference, ΔP. The cell membrane is impermeable to the solute, but water permeates through the membrane with a normal velocity $\nu \cdot \mathbf{u}_f$. Therefore the membrane must move with equal and opposite velocity $-\nu \cdot \mathbf{u}_f$. This fact gives the following interface conditions for the solute on the cell boundary:

$$\tau \cdot \mathbf{u}_f(\mathbf{x}, t) = 0, \quad \mathbf{x} \in \partial\Omega(t), \tag{2.9}$$

$$\nu \cdot \mathbf{u}_f(\mathbf{x}, t) = LRT\Delta c(\mathbf{x}, t), \quad \mathbf{x} \in \partial\Omega(t), \tag{2.10}$$

$$D\frac{\partial c}{\partial \nu} = \nu \cdot \mathbf{u}_f \cdot c(\mathbf{x}, t), \quad \mathbf{x} \in \partial\Omega(t). \tag{2.11}$$

The other boundary conditions applied on the outer computational domain is the Dirichlet boundary condition for c field and the Neumann boundary condition for $\mathbf{u}$. In a homogeneous external medium, these interface conditions lead to the shrinking of cells for hypertonic environment ($\nu \cdot \mathbf{u}_f > 0$) and to the swelling of cells in the hypotonic case ($\nu \cdot \mathbf{u}_f < 0$), and thus they represent osmosis. Our natural convection model is described by the coupled equations that consist of the convection-diffusion for concentration field (2.2), the fluid momentum equations (2.5),(2.8) and the cell interface conditions (2.9), (2.10), and (2.11). The boundary conditions for concentration and velocity fields in computational boundary domain are given as neumann conditions. These equations can be made in dimensionless forms by introducing reference values. In free convection, there is no easily available reference velocity. Therefore, instead of using it, the ratio $\mu/\rho l$ has been used for U with following dimensionless variables:

$$\mathbf{u}^* = \mathbf{u}_f l\rho/\mu, \quad t^* = \frac{\mu t}{\rho l^2}, \quad c^* = \frac{c - c_B}{c_f - c_B},$$

where μ, l, and $c_f - c_B$ are the dynamic viscosity, characteristic length, and characteristic concentration difference in the system, respectively. The resulting dimensionless equations are then given by

$$\begin{aligned} \nabla^* \cdot \mathbf{u}^* &= 0, && (2.12)\\ \frac{\partial c^*}{\partial t^*} + \mathbf{u}^* \cdot \nabla^* c^* &= \frac{1}{Sc} \nabla^{*2} c^*, && (2.13)\\ \frac{\partial \mathbf{u}^*}{\partial t^*} + (\mathbf{u}^* \cdot \nabla^*)\mathbf{u}^* &= \nabla^{*2}\mathbf{u}^* - c^* Gr \frac{\mathbf{g}}{g}, && (2.14) \end{aligned}$$

where $Sc = \nu/D$, $Gr = \rho^2 \mathbf{g} l^3 (c_f - c_B)/\mu^2 \cdot 1/\rho(c_B) \cdot (\partial\rho/\partial c)_{c_B}$ are the Schmidt number and the Grashof number for mass transfer.

Similarly, the dimensionless interface conditions are given by

$$\begin{aligned} \tau \cdot \mathbf{u}^*(\mathbf{x}, t) &= 0, && (2.15)\\ \nu \cdot \mathbf{u}^*(\mathbf{x}, t) &= \frac{LRTl(c_f - c_B)}{\nu} \Delta c^*(\mathbf{x}, t), && (2.16)\\ D \frac{\partial c^*}{\partial \nu} &= LRTl\, \nu \cdot \mathbf{u}^* c^*(\mathbf{x}, t). && (2.17) \end{aligned}$$

After computing all the concentration field, velocity field and membrane movement velocity, we shall use the level set technique to "capture" the interface as in [21]. Our level set function is denoted as ϕ and it is taken positive outside the cell and negative inside the cell. Therefore, the interface of the semi-permeable membrane cell is the zero level set of ϕ, that is the set of points of $\phi = 0$. In our algorithm, we initialize ϕ as the signed distance function from the interface. And solving the level set equation,

$$\phi_t + \mathbf{u}_m \cdot \nabla\phi = 0, \tag{2.18}$$

we can track the interface of cell membrane from the zero level set of ϕ. This equation (2.18) moves the zero level set of ϕ exactly as the actual cell interface moves.

3. Algorithm

3.1. **Flow chart.** Firstly, we begin by looking at the brief flow chart and move on in details.

- **Step 1.** Initialize $\phi(\mathbf{x}, 0)$ to be the signed normal distance to the cell membrane.
- **Step 2.** Solve the momentum equation, the transport equation and the level set equation for one time step to get $\mathbf{u}_f(\mathbf{x}, t + \Delta t)$, $c(\mathbf{x}, t + \Delta t)$ and $\phi(\mathbf{x}, t + \Delta t)$.
- **Step 3.** We have now advanced one time step. The zero level set of $\phi(\mathbf{x}, t + \Delta t))$ gives the new interface position of semi-permeable membrane.
- Repeat Steps 2 and 3 until the natural convection flow reaches the steady state.

In Step 3, the computation will be declared to have reached steady state when either the relative change in the L_2 norm of the time step velocity difference is less than input tolerance,

$$\frac{\sqrt{\sum_x |\mathbf{u}_f(\mathbf{x}, t + \Delta t) - \mathbf{u}_f(\mathbf{x}, t)|^2}}{\sqrt{\sum_x |\mathbf{u}_f(\mathbf{x}, t)|^2}} \leq tol, \tag{3.1}$$

or the relative error in the intra and extracellular average concentrations are less than input tolerance,

$$\left| \frac{\sum_{x_f} c_f/N_f - \sum_{x_c} c_c/N_c}{\sum_{x_f} c_f/N_f} \right| \leq tol, \tag{3.2}$$

where N_f, N_c are numbers of nodes in extra and intracellular regions, respectively.

3.2. **Discretization.** $M \times N$ rectangular mesh will be used for the numerical simulation. With h as the mesh size, we define for $i = 0, ..., M-1, j = 0, ..., N-1$,

$$\mathbf{x}_{i,j} = (ih, jh), \quad \mathbf{u}_{i,j} = \mathbf{u}(\mathbf{x}_{i,j}), \quad c_{i,j} = c(\mathbf{x}_{i,j}), \quad \phi_{i,j} = \phi(\mathbf{x}_{i,j}),$$

where M, N are the number of grids in each $x-, y-$ direction.

From this section, $\mathbf{u}$ represents $\mathbf{u}_f$ unless otherwise stated.

(1) Discretization of the transport equation.
We will use the first order forward Euler scheme to evolve in time

$$\frac{c^{n+1} - c^n}{\Delta t} = -(\mathbf{u}^n \cdot \nabla)c^n + D\nabla^2 c^n, \tag{3.3}$$

where Δt is the time step size. We will use the second order central difference scheme for the approximation of the convection and diffusion terms in the transport equation. On the interface (semi-permeable membrane), the second order central difference scheme with the interface condition will be implemented.

(2) Discretization of the momentum equation.
With updating the concentration field in Equation (3.3), we also use the second order central difference scheme for the approximation of the convection and diffusion terms in the momentum equation. On the interface, a second order central difference scheme with interface condition is implemented.

$$\frac{\mathbf{u}^{n+1} - \mathbf{u}^n}{\Delta t} = -(\mathbf{u}^n \cdot \nabla)\mathbf{u}^n + \frac{\mu}{\rho(c_B)}\nabla^2 \mathbf{u}^n + \frac{\mathbf{g}}{\rho(c_B)}(\frac{d\rho}{dc})_{c_B}(c_B - c^{n+1}). \tag{3.4}$$

(3) Discretization of the level set equation.
When we solve for level set equation, we need to compute approximations to the spatial derivatives of ϕ.

$$\phi_t = -\mathbf{u}_m \cdot \nabla\phi = \mathcal{R}(\phi), \tag{3.5}$$

where $\mathcal{R}$ is the spatial differential operator of the level set equation. We use the first order Godunov's scheme or a third-order ENO approximations. For the temporal discretization of the equation, we use a simple forward Euler or the following third order TVD-Runge-Kutta type time discretization. The time discretization for Equation (3.5)

is

$$\begin{aligned}\phi^{(1)} &= \phi^{(0)} + \Delta t R(\phi^{(0)}),\\ \phi^{(2)} &= \frac{3}{4}\phi^{(0)} + \frac{1}{4}\phi^{(1)} + \frac{1}{4}\Delta t R(\phi^{(1)}),\\ \phi^{(3)} &= \frac{1}{3}\phi^{(0)} + \frac{2}{3}\phi^{(2)} + \frac{2}{3}\Delta t R(\phi^{(2)}),\end{aligned}$$

where R is the discrete approximation to $\mathcal{R}$. Denote the updated ϕ by ϕ^{n+1}.

(4) Reinitialization of the distance function.
To make sure that $\phi(\mathbf{x}, t)$ is a signed distance function, we construct a new distance function ψ by solving

$$\psi_t = S(\phi^{n+1})(1 - |\nabla\psi|) \tag{3.6}$$

with $S(\phi) = \frac{\phi}{\sqrt{\phi^2+\epsilon^2}}$ until we reach a steady state solution ψ. This steady state solution ψ is then used to replace ϕ^{n+1}, again denoted by ϕ^{n+1}.

We have used the following discretization to evolve Equation (3.6). Define

$$\begin{aligned}a &= D_x^-\psi_{i,j} = (\psi_{i,j} - \psi_{i-1,j})/h,\\ b &= D_x^+\psi_{i,j} = (\psi_{i+1,j} - \psi_{i,j})/h,\\ c &= D_y^-\psi_{i,j} = (\psi_{i,j} - \psi_{i,j-1})/h,\\ d &= D_y^+\psi_{i,j} = (\psi_{i,j+1} - \psi_{i,j})/h,\end{aligned}$$

and

$$G(\psi_{i,j}) = \begin{cases}\sqrt{(\max((a^+)^2, (b^-)^2) + \max((c^+)^2, (d^-)^2)} - 1, & \text{if } \psi^0_{i,j} > 0,\\ \sqrt{(\max((a^-)^2, (b^+)^2) + \max((c^-)^2, (d^+)^2)} - 1, & \text{if } \psi^0_{i,j} < 0,\\ 0, & \text{otherwise,}\end{cases}$$

where $+$ and $-$ represent the positive and negative parts, respectively. Now, we update (3.6) using

$$\psi^{n+1}_{i,j} = \psi^n_{i,j} - \Delta t S(\phi_{i,j}) G(\psi^n_{i,j}). \tag{3.7}$$

The stopping criterion for the iteration is given by

$$\frac{\sum_{|\psi^n_{i,j}|<\alpha} |\psi^{n+1}_{i,j} - \psi^n_{i,j}|}{N} < \Delta t h^2,$$

where N is the number of grid points where $|\psi^n_{i,j}| < \alpha$. Usually, $\Delta t = h/5$, $\epsilon = h$ have been chosen during the computation. Then Equation (3.7) guarantees that ψ is a signed normal distance function [18].

(5) Computation of Δt.
During the implementation, the time step must satisfy the CFL conditions due to the convective and diffusive terms in Equation (3.3). Also due to convective and viscous

terms in Equation (3.4), restrictions on the time step are imposed to satisfy the following conditions:

$$\Delta t_c \equiv \frac{h}{\max|u|}, \quad \Delta t_d \equiv \frac{h^2}{D}, \quad \Delta t_v \equiv \frac{h^2}{\nu}, \quad \Delta t^{n+1} = 0.5\min(\Delta t_c, \Delta t_d, \Delta t_v).$$

4. NUMERICAL RESULTS

We have validated our method considering the following problems. In the numerical examples, we use the following constants unless otherwise specified ($D = 1\mu m^2/s$,$\nu = 1\mu m^2/s$, $LRT = 1\mu m/s \cdot M$, $\mathbf{g}$ is ignorable.). Consider a computational domain $10\mu m \times 10\mu m$ in the case of Examples 1 and 2. The domain is initially filled with sodium water with different concentration value and the governing equations are following:

$$\begin{aligned}
\nabla \cdot \mathbf{u} &= 0, && (4.1)\\
\frac{\partial c}{\partial t} &= D\nabla^2 c - \mathbf{u}\cdot\nabla c + a, && (4.2)\\
\frac{\partial \mathbf{u}}{\partial t} + (\mathbf{u}\cdot\nabla)\mathbf{u} &= \frac{\mu}{\rho}\nabla^2\mathbf{u} + \frac{1}{\rho(c_B)}\mathbf{g}\left(\frac{d\rho}{dc}\right)_{c_B}(c_B - c) + \mathbf{f}, && (4.3)\\
\phi_t - \mathbf{u}\cdot\nabla\phi &= 0, && (4.4)\\
\tau\cdot\mathbf{u} &= 0, && (4.5)\\
\nu\cdot\mathbf{u}(\mathbf{x},t) &= LRT\Delta c(\mathbf{x},t) + b1, && (4.6)\\
D\frac{\partial c}{\partial \nu} &= \nu\cdot\mathbf{u}\cdot c(\mathbf{x},t) + b2, && (4.7)
\end{aligned}$$

where $a(\mathbf{x},t)$, $\mathbf{f}(\mathbf{x},t) = (f_1(\mathbf{x},t), f_2(\mathbf{x},t)), b_1, b_2$ are source terms which are generated by exact solutions. For typical biological system the values of the physical parameters are : $l \approx 1 - 10\mu m, c = 5\times 10^{-10} mol/m^3, \mu = 10^{-3} N\cdot s/m^2, T = 300K, L = 10^{-11} m^3/N\cdot s, \gamma = 10^{-3} N/m$. Let us convert the units to $g, \mu m, s$ and list them on the following table.

The Grashof number represents the relative importance of the buoyancy forces with respect to the viscous forces.The influence of this number on the shape of the free boundary, the concentration distribution and the flow field is shown in figures (in numerical results). In general, for large values of the Grashof number, the convective terms in the Navier-Stokes equations dominate the diffusive terms and finer grid is necessary in order to take into account the velocity boundary layer near the cell membrane. Since the Grashof number appears on the right-hand side of the second component of the Navier-Stokes equations, the corresponding buoyancy force acts on the fluid particles in upward direction.A large Gr indicates a large concentration gradient in the boundary layer of the membrane, and hence a larger effect of natural convection on performance.

TABLE 1. Units and Values in Experiments

Parameters	Units	Values
L (hydraulic permeability)	$\mu m/min \cdot atm, m^3/N \cdot s$	0.001644 $\mu m^2 \cdot s/g$
R (universal gas constant)	$atm/M \cdot K, N \cdot m/K \cdot M$	8.3147 $g/s^2 \cdot \mu m \cdot M \cdot K$
T (absolute temperature)	K(kelvin)	300 K
γ (surface tension)	N/m	1 g/s^2
κ (curvature)	$1/(\mu m)$	
D (diffusivity)	$\mu m^2/s$	7.8-7800 $\mu m^2/s$
μ (dynamic viscosity)	$N \cdot s/m^2, g/s \cdot \mu m$	$10^{-6} g/s \cdot \mu m$, $(\nu) 1 - 10^4$
C (concentration)	mol per liter	1 M
l (cell radius)	μm	$3\mu m$
g' (gravity factor)	$\mu m \cdot s^2/M$	$10^{-4} - 10^3$

4.1. **Example 1: Continuous concentration field.** Consider the following solutions for Equations (4.1)–(4.7):

$$\begin{aligned} u(x,y,t) &= -0.5\frac{e^{-t}}{x^2+y^2}\begin{pmatrix} x \\ y \end{pmatrix}, \quad (x,y) \in \Omega_c \cup \Omega_f, \\ c(x,y,t) &= c^{eq} + \frac{e^{-t}}{1+x^2+y^2}, \quad (x,y) \in \Omega_c \cup \Omega_f. \end{aligned}$$

In the numerical test, c^{eq} is an equilibrium value and taken as 262.5 Mols. Then, the corresponding source terms are generated by the above solutions.

Initially, the concentration value at the center point is the highest and it has decreasing values as it goes far away from the center. Since the velocity at the center is not defined, we set the center velocity value as the maximum velocity near the center. After 0.3 seconds, the relative concentration error between the averages of intracellular and extracellular concentration values is less than given tolerance. These validation computations were done in single precision; the value of tol was set to 10^{-3}. The exact and numerical concentration and velocity fields are shown in Figure 1. Figure 2 (a) compares the level curves of initial state and state after 0.3sec. Since there is no gravity and forcing factor except concentration difference, the cell only swells having the same center at all times. For a convergence test, we have tested with various meshes ($h = 0.2$, $h = 0.1$, $h = 0.05$), and plotted the relative errors in velocity in Figure 2 (b). The numerical convergence accuracy in this simmulation is about 1.4. Even though we implemented the second order scheme for the space discretization, the scheme applied to interface and boundary decreases the whole order of accuracy.

4.2. **Example 2: Discontinuous concentration field.** As a second example, consider the case where the concentration field is discontinuous. The exact solutions for (4.1)-(4.7) are obtained

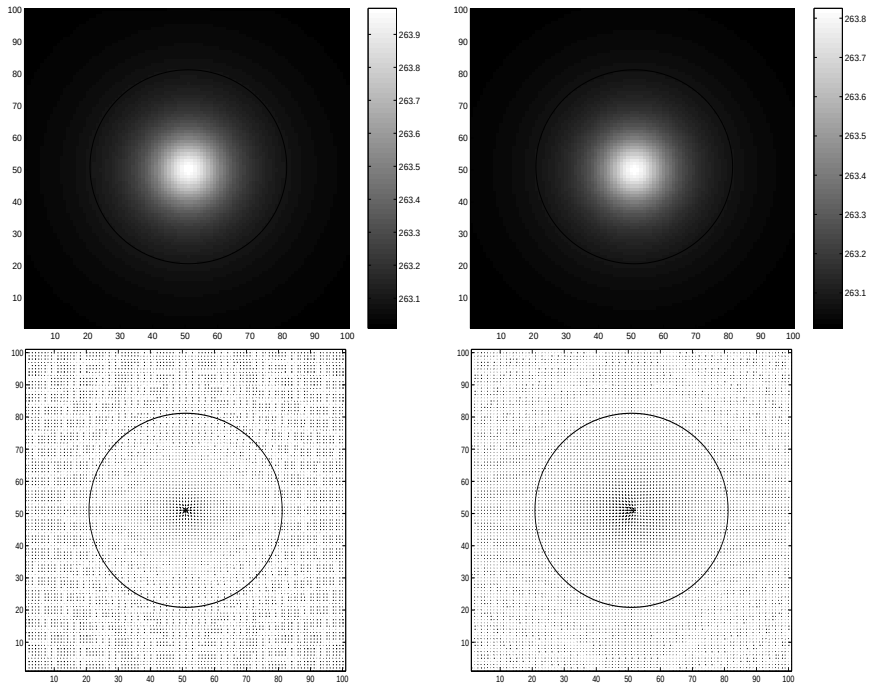

FIGURE 1. Concentration and velocity field at the steady state under continuous concentration field at 0.3 sec.: (a) analytic concentration, (b) concentration obtained by numerical experiment, (c) analytic velocity field, (d) velocity field obtained by numerical experiment. Computational geometry is $10\mu m \times 10\mu m$, and $h = 0.1$. Solid curves in each figures represent the cell membrane interface.

as follows. Corresponding source terms are generated by the exact solutions:

$$\begin{aligned} u(x,y,t) &= -0.5\frac{e^{-t}}{x^2+y^2}\begin{pmatrix} x \\ y \end{pmatrix}, \qquad (x,y) \in \Omega_c \cup \Omega_f, \\ c(x,y,t) &= \begin{cases} c_c - (1-e^{-t})(1+x^2+y^2), & (x,y) \in \Omega_c, \\ c_f + \frac{100(1-e^{-t})}{1+x^2+y^2}, & (x,y) \in \Omega_f, \end{cases} \end{aligned}$$

where c_c and c_f represent intracellular and extracellular concentrations and initially set as 290 Mols and 235 Mols. As time proceeds, the average value of outside concentration is increasing and the average value of inside concentration is decreasing. After 0.35 seconds, the relative concentration error does not change, therefore we arrive at the steady state solution. The exact and numerical concentration and velocity fields are shown in Figure 3. Due to the effect of a solute concentration difference on the osmotic stress, water rushes in to the area of high solute concentration, enlarging the cell. The level curves are shown in Figure 4(a). For a convergence

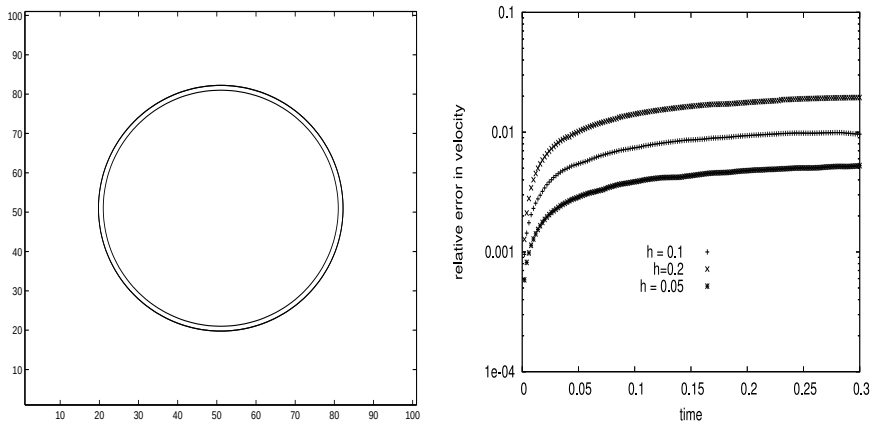

FIGURE 2. These results were calculated under continuous concentration field at 0.3 sec. (a) The initial level curve (inner circle) and the level curve (outer circle) at time =0.3 sec. The computational geometry is $10\mu m \times 10\mu m$, and $h = 0.1$. (b) The relative errors of velocity field in L_2 norm according to various mesh spacings.

test, we have tested with various meshes ($h = 0.2$, $h = 0.1$, $h = 0.05$), and have plotted the relative errors in velocity in Figure 4 (b) which shows a good convergence result.

4.3. **Example3: Erythrocytes.** In the case of $Gr = 0$, the osmotic swelling of a cell is simulated by imposing a uniform concentration values between the inner and outer solutions. At first, a circle cell(spherical-like) is considered, where only a change of volume is expected with the shape remaining unaltered. Figure shows the evolution of various variables under the effects of different initial osmotic loads, $c_{in} - c_{out}$. In order to assess the practical importance of the natural convection driven model by osmosis, we examine the realistic biophysical values with various parameter values. A human biconcave erythrocyte (red blood cell) is described as

$$(x^2 + y^2 + z^2)^2 + P(x^2 + y^2) + Qz^2 + R = 0, \tag{4.8}$$

where $P = -15.3\mu m^2, Q = 42.0\mu m^2, R = -10.6\mu m^4$.

In this example, we make a couple of assumptions, erythrocytes are far from each other so that we can consider a single cell model. The shape of erythrocyte may be described as a biconcave disc as in (4.8) , but for simplicity, we choose to represent the erythrocyte as a simple disc-shaped cell with a constant surface area as well as the case of biconcave cell. This simplifying assumption is supported by the experimental observation in [3]. The simulation of osmotic phenomena can be performed by considering realistic values for the various parameters. The permeability of RBC is in the range of 4-10 $\mu m/min \cdot atm$, around $10^{-6}\mu m/s \cdot Pa$ and a mean radius is about 3-5 μm. We have chosen the radius 3 μm circle for our cell in the $32\mu m \times 32\mu m$ computational domain. The grid size in each direction chosen here is 0.1 μm. We have used the temperature of water $T = 273K$, the universal gas constant $R = 0.08206 atm/\mathrm{Mol} \cdot K$ and the

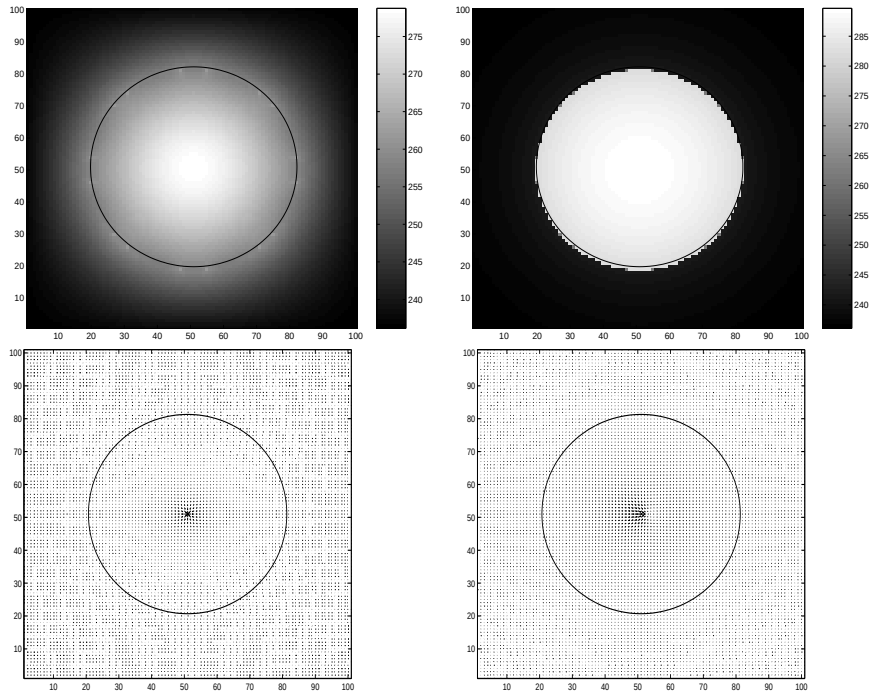

FIGURE 3. Concentration and velocity fields at the steady state under discontinuous concentration field: (a) analytic concentration, (b) concentration obtained by numerical experiment, (c) analytic velocity field, (d) velocity field obtained by numerical experiment. Computational geometry is $10\mu m \times 10\mu m$, and $h = 0.1$. Solid curves in each figures represent the cell membrane interface.

hydraulic permeability $L = 10\mu m/min \cdot atm$, respectively. The concentration values in the intra and extra of the cell are given 140Mol and 93.6Mol respectively as in [5]. The diffusivity D is $780\mu m^2/s$ and the membrane permeability is $P = LRT = 4.03\mu m/s \cdot \text{Mol}$. The kinematic viscosity ν varies from 1 $\mu m^2/s$ to 10000 $\mu m^2/s$. The related numerical computations are shown in following figures.

Let us first assume that there is no affecting gravitational force. This is reasonable when we are specially dealing with micro-nano bio-cell membranes. Figure 5 (a) shows the concentration field at steady state. In the beginning of the simulation, there is an apparent concentration gradient between the intra and extra of cell but at the steady state the concentrations converge. Two solid curves represent level curves of initial (inner) and steady state (outer). In Figure 5 (b), we have plotted that the average concentration values in the intra and extra of the cell and observed that concentration outside of a cell is decreasing and concentration inside of cell is gradually increasing thus they reach the steady state. Figure 5 (c) shows the velocity field at

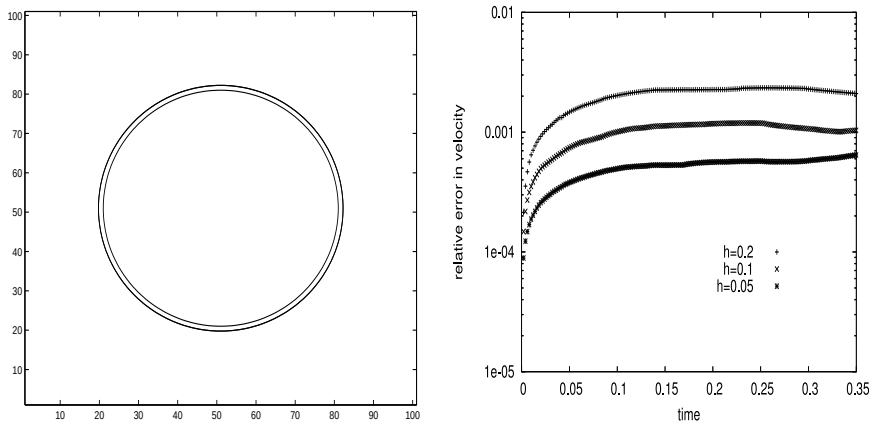

FIGURE 4. These results was calculated under discontinuous concentration field. (a) The initial level curve (inner circle) and level curve (outer circle) at time =0.3 sec. The computational geometry is $10\mu m \times 10\mu m$, and $h = 0.1$. (b) The relative errors of velocity field in L_2 norm according to various mesh spacings.

steady state within $|\phi(x,t)| < 5h$, two solid curves are level curves of initial (inner) and steady state (outer). In Figure 5 (d), we have plotted the graph of the maximum velocity values.

Now, we take into account of a gravitational force. The gravity factor $\mathbf{g}' = \frac{\mathbf{g}}{\rho(c_B)}(\frac{d\rho}{dc})_{c_B} = (0, 100\mu m \cdot s^2/\mathrm{Mol})$ is assumed. Figure 6 (a) shows the concentration field at steady state. In the beginning of the simulation, there is an apparent concentration gradient between the intra and extra of a cell, but at the steady state, the concentrations converge. Two solid curves represent level curves of initial (inner) and steady state (outer). With the presence of gravity, the cell not only swells but also migrates in the direction where the gravity force applies. In Figure 6 (b), we have plotted the average concentration values in the intra and extra of the cell and observed that the concentration outside the cell is decreasing and that inside the cell is gradually increasing until they reach the steady state. Figure 6 (c) shows the velocity field at steady state within $|\phi(x,t)| < 5h$, two solid curves are level curves of initial (inner) and steady state (outer). In this figure, we observed some numerical instability on the interface, ENO or WENO scheme for space discretization could be one method to overcome this phenomena. In Figure 6 (d), we have plotted the graph of the maximum velocity values. However, when the viscosity value is above 1000 $\mu m^2/s$, the membrane movement is ignorable.

As a final numerical result, we demonstrate the case of two dimensional biconcave shape cell as given in Equation (4.8). The bulk concentration is 21 Mol, and the initial intracellular concentration is 114.5 Mol. The computational domain is $16\mu m \times 32\ \mu m$ and the grid size in each direction is 0.1 μm. The diffusivity D is $780\mu m^2/s$, the membrane permeability $P = LRT = 4.03\mu m/s \cdot M$, the kinematic viscosity 1 $\mu m^2/s$, and the gravity factor is assumed to be zero. In Figure 7 (a), two solid curves represent the level curves at initial(inner)

and steady state(outer). In Figure 7 (b), we have plotted the average concentration values in the intra and extra of the cell and observed that the concentration outside the cell is decreasing and that inside the cell is gradually increasing until they reach the steady state. Figure 7 (c) shows the fluid velocity field at steady state within $|\phi(x,t)| < 5h$. The RBC is initially set as hypotonic condition, thus we can observe that fluid movement from the extracellular region into the RBC cell which makes the cell swell. In Figure 7 (d), we have plotted the graph of the maximum velocity values.

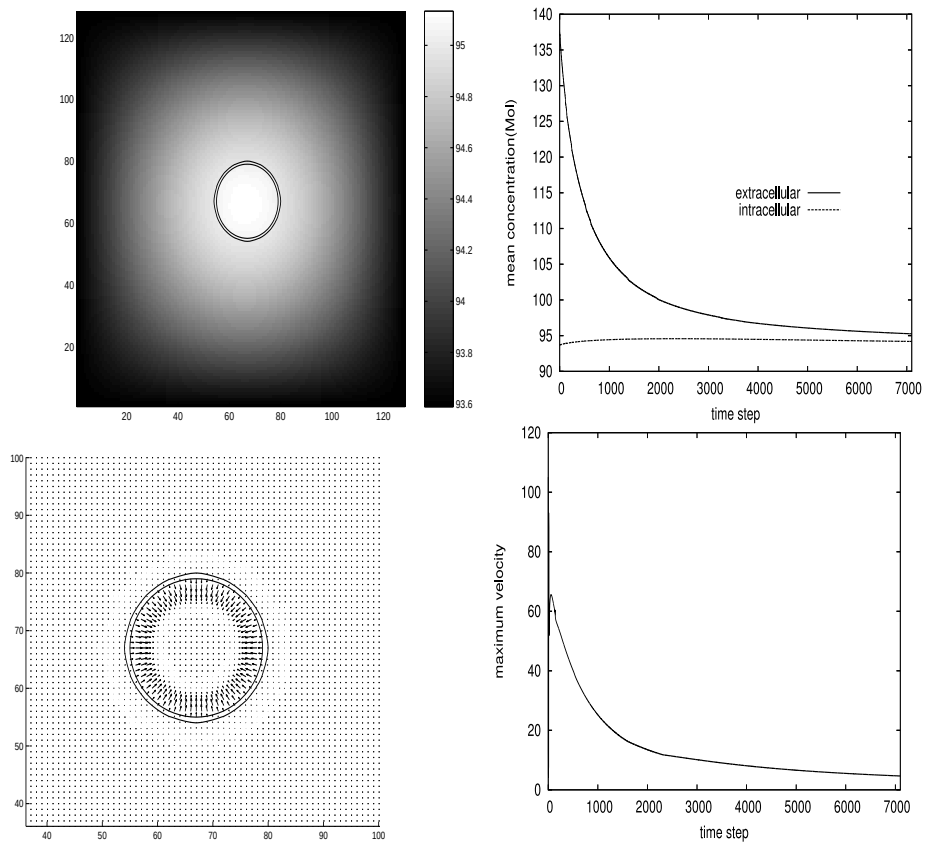

FIGURE 5. A simple circle erythrocyte model, (a) Concentration field at steady state, two solid curves are level curves of RBC; inner and outer circles at the initial and steady states. (b) The plot of average concentration value versus time iteration (c) The enlarged velocity field at steady state (right) within $|\phi(x,t)| < 5h$, two solid curves are level curves of RBC; inner and outer circles at initial and steady state. (d) The plot of maximum velocity versus time. The computational geometry is $32\mu m \times 32\mu m$ with the mesh $h = 0.25$.

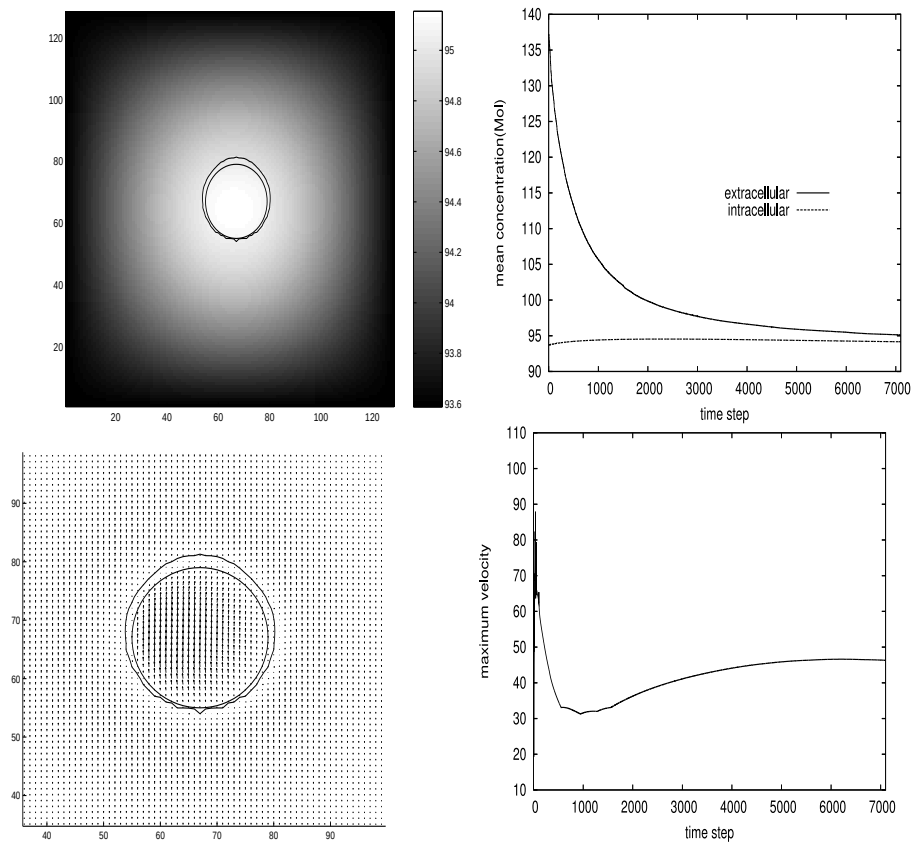

FIGURE 6. A simple circle erythrocyte model with gravity, (a) Concentration field at steady state, two solid curves are level curves of RBC; inner and outer circles at initial and steady state. (b) The plot of average concentration value versus time iteration (c) The enlarged velocity field at steady state (right) within $|\phi(x,t)| < 5h$, two solid curves are level curves of RBC; inner and outer circles at initial and steady state. (d) The plot of maximum velocity versus time. The computational geometry is $32\mu m \times 32\mu m$ with the mesh $h = 0.25$.

5. CONCLUSIONS

In this paper, we have discussed about the transport phenomena across a semi-permeable membrane. Unlike an ionic transport across a membrane, the variables are macroscopic concentration and velocity fields. Considering the semi-permeable interface condition, we have established the coupled transport and Navier-Stokes equation which describe the osmotic phenomena. In section 3, we have designed the numerical algorithm to simulate our osmotic model. Verification studies were performed by constructing the exact solutions in the case

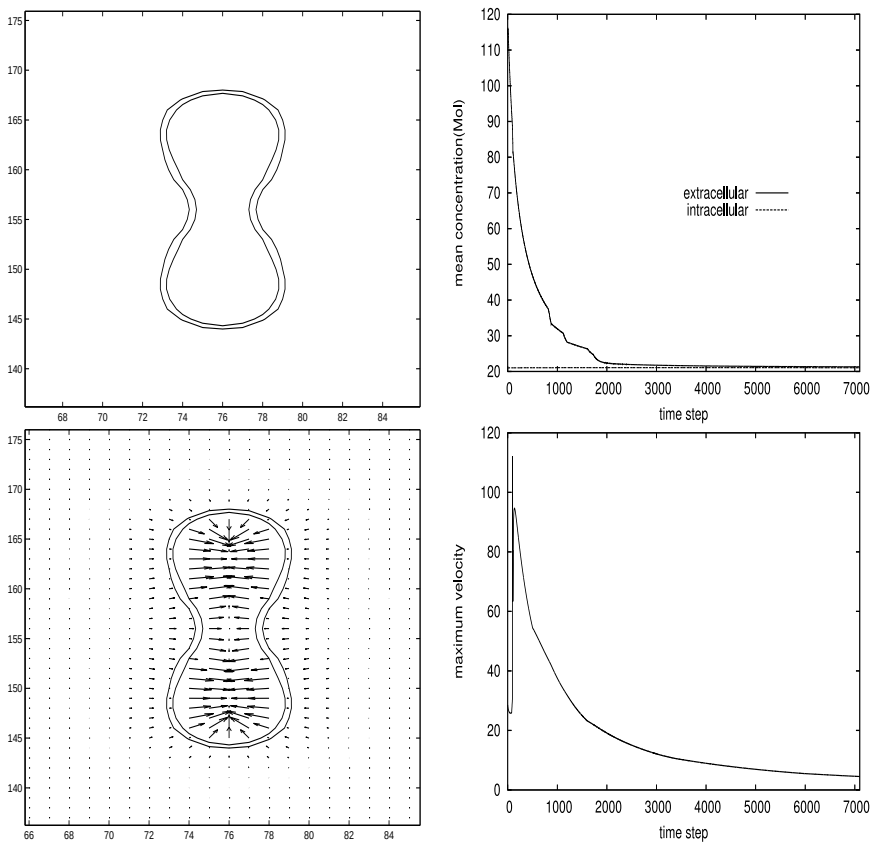

FIGURE 7. A biconcave erythrocyte model. (a) Level curves at initial and steady state. (b) The plot of average concentration value versus time iteration (c) Velocity field at steady state . (d) The plot of maximum velocity versus time. The computational geometry is $16\mu m \times 32\mu m$ with the mesh $h = 0.1$.

of continuous, discontinuous concentration fields. Our results indicate that our method can predict the cell movement in hypotonic solution. Similar simulations on simple erythrocyte geometry were studied in section 4. Most studies on osmotic phenomena are described by simple diffusion-type equations ignoring all fluid motion, thus are interested in obtaining concentration field. In our work, we could get not only the concentration field but also the velocity field over the domain tracking the cell membrane interface.

ACKNOWLEDGEMENT

This work was supported by a grant of the Korean Research Foundation KRF-2006-070-C00014.

REFERENCES

[1] J.L. Anderson. Movement of a semi-permeable vesicle through an osmotic gradient. *Phys. Fluids*, 26:2871–2879, 1983.

[2] R.P. Batycky, R. Hammerstedt, and D.A. Edwards. Osmotically driven intracellular transport phenomena. *Phil. Trans. R. Soc. Lond. A.*, 355:2459–2488, 1997.

[3] E. Evans and Y.C. Fung. Improved measurements of the erythrocyte geometry. *Microvasc. Res.*, 4:335–347, 1972.

[4] R.H. Hammerstedt, J.K. Graham, and J.P. Nolan. Cryopreservation of mammalian sperm: what we ask them to survive. *J. Androl.*, 11:73–88, 1990.

[5] M. Jaeger, M. Carin, M. Medale, and G. Tryggvason. The osmotic migration of cells in a solute gradient. *Biophys. J.*, 77:1257–1267, 1999.

[6] T. Khan and P.M. Reppert. A finite element simulation of frequency-dependent electro-osmosis. *J. Colloid and Interface Science*, 290:574–581, 2005.

[7] N.B. Kirichenko. Natural convection in a horizontal in a non-flow-through reverse-osmosis cell. *Theoretical foundations of chemical engineering*, 39:310–318, 2005.

[8] R.L. Levin, E.G. Cravalho, and C.E. Huggins. Effect of hydration on the water content of human erythrocytes. *Biophy. J.*, 16:1411– 1426, 1976.

[9] S.K. Li, A.H. Ghanem, and W.I. Higuchi. Pore charge distribution considerations in human epidermal membrane electroosmosis. *J. Pharm. Sci.*, 88:1044–1049, 1999.

[10] J. Liu, J.A. Christian, and J.K. Critser. Canine RBC osmotic tolerance and membrane permeability. *Cryobiology*, 44:258–268, 2002.

[11] R. Madhusudan, J. Lin, and S. Murad. Molecular simulation of osmosis, reverse osmosis and electro-osmosis in fluid mixtures using semi-permeable membranes. *Fluid phase equilibria*, 150-151:97–105, 1998.

[12] P. Mazur. Freezing of living cells: mechanisms and implications. *Amer. J. Physiol.*, 247:C125–C142, 1984.

[13] P. Mazur, W.F. Rall, and S.P. Liebo. Kinetics of water loss and likelihood of intracellular freezing in the mouse ova. *Cell Biophys.*, 6(3):197–213, 1984.

[14] S. Murad, K. Oder, and J. Lin. Molecular simulation of osmosis, reverse osmosis and electro-osmosis in aqueous and methanolic electrolyte solutions. *Molecular Physics*, 95(3):401–408, 1998.

[15] S. Murad and J.G. Powels. Computer simulation of osmosis and reverse osmosis in solutions. *Chem. Phys. Lett.*, 225:437–440, 1994.

[16] T.J. Pedley. Natural convection driven by osmosis. *SIAM J. Appl. Math.*, 42(6):1202–1216, 1982.

[17] P.J. Quinn. A lipid-phase separation model of low temperature damage to biological membranes. *Cryobiol.*, 22:128–146, 1989.

[18] E. Rony and A. Tourin. A viscosity solutions approach to shape-from-shading. *SIAM J. Numer. Anal.*, 29(3):867–884, 1992.

[19] S. Shiba, S. Hino, Y. Hirato, and T. Seno. Removal of heavy metal from soil and groundwater by in-situ electrokinetic remediation. *Water Sci. Technol.*, 42(7-8):335–343, 2000.

[20] S. Sourirajan. *Reverse Osmosis*. Academic Press, New York, 1970.

[21] M. Sussman, P. Smereka, and S. Osher. A level set approach for computing solutions to incompressible two-phase flow. *J. Comp. Phys.*, 114:146–159, 1994.

[22] K. Zhou and L. Song. Experimental study of water and salt fluxes through reverse osmosis membranes. *Environ. Sci. Technol.*, 39:3382–3387, 2005.

[23] D. Zinemanas and A. Nir. Osmophoretic motion of deformable particles. *Int. J. Multiphase Flow*, 21:787–800, 1995.